- Technical Paper -

PRELIMINARY PUSH-OUT TEST AND FE ANALYSIS OF PERFORATED SHEAR CONNECTORS FOR REUSABLE STRUCTURAL ELEMENTS

Hassane OUSALEM[*1], Satoshi KAKE[*2]

ABSTRACT

Aiming for suitable joints of reusable structural elements, the strength of perforated steel plates used as shear connectors welded to beam top flange and connected to concrete slab is investigated experimentally and numerically. Two types of joints were compared: Shear connectors when embedded directly in a concrete slab and shear connectors embedded in grouted pockets made in the slab. Test results showed the suitability of the latter type in terms of strength, deformation, ductility and stiffness. The numerical investigation proved to be appropriate in evaluating the behavior of such connectors.
Keywords: precast construction, reusable structure, shear connector, push-out test, numerical analysis

1. INTRODUCTION

Aiming sustainability for greener construction to preserve the environment, contributors in that field are gradually undertaking challenging steps to set their activities into the orbit of circular economy [1]. Whereas various precast structural systems for rapid construction and quality insurance [2-3] were conceived, a decade ago, structural concrete elements' re-using options were, in most cases, ignored during the design and development of structures. Recently, demountable connections at different locations of structures have gradually been developed and various configurations have been implemented, particularly for beam-slab connections [4].

A demountable/reusable beam-slab system (Fig.1) using burring-process perforated steel plates (Fig.2) as shear connectors is introduced. It enables reuse of structural members without causing any damage to them during dismantling. For assembling, after placing a precast slab with circular pockets (holes) on the beam with the shear connectors installed, the circular pockets are filled with grout to integrate the slab with the beam. For dismantling, the circular pockets' grout is cored and separated from the slab, and then the slab is lifted. Before stocking/reusing the slab, the wall of the cored pocket should be treated to insure, for a future use, a good bond between slab concrete and the new grout.

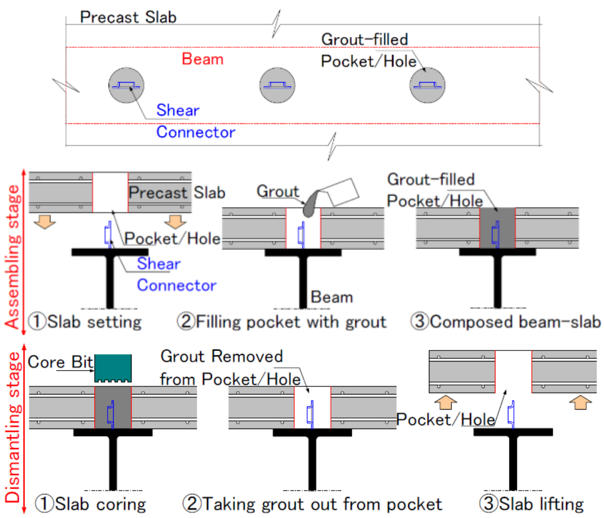

Fig.1 Demountable/reusable beam-slab system

The shear connector is made by burring process to increase the bearing contact area and consequently prevent high stress concentration compared to the stud/bolt option. As the proposed connector is less flexible and has higher moment of inertia than stud/bolt connector, under a similar load level, a small number of the proposed connector can be used instead. As the proposed construction method of the floor system relies only on the grout junction at the shear connector, no load transfer is expected to occur along the beam and slab mutual faces, except at the locations of the shear connectors. Consequently, a complete uniform behavior between the beam part and the slab part becomes questionable, and the performance of the proposed structural system should be investigated. In this paper, as a preliminary study, only the connection is examined by comparing the conventional practice of the mentioned shear connectors when embedded directly in a concrete slab [3] to the case when they are embedded in grouted pockets made in the slab. This study investigated, experimentally by push-out tests and numerically by FE modeling, the composite behavior of such shear connectors under static shear loading.

2. PUSH-OUT TEST

2.1 Specimens and materials

To determine the characteristics of the proposed shear connection, a typical monotonic push-out test was carried out on two types of specimens (BR-N type and BR-P type). The BR-N type represents the conventional construction method (cast-in place slab, non-demountable elements) where the concrete is cast directly on the beam with the connectors. The BR-P represents the proposed construction method (precast slab, demountable elements). Three identical specimens

*1 Chief Researcher, TAKENAKA Research & Development Institute, Ph.D., JCI Member
*2 Researcher, TAKENAKA Research & Development Institute, M.E., JCI Member

were constructed for each type. Figure 2 shows the dimensions of specimens and their detailing, and Table 1 shows their list. Diameter of the grouted pocket was conditioned by the connector size. By presuming that the connector's burring part would mainly bear all loadings and aiming to reduce the amount of the grout, in this preliminary investigation, the pocket diameter was set to 130mm. To prevent any concrete-steel bond/friction and measure only the bearing strength of the shear connector, 2 layers of Teflon sheets were set on each steel T-beam before casting/setting concrete blocks. Burring-process perforated shear connector was made from a 6mm-thick steel plate (SN400B material type) and had a height and hole diameter of 100 mm and 50 mm, respectively, and was welded to a T-section rolled steel beam (SS400 material type). Each concrete block was allocated with one shear connector. Slightly reinforced concrete blocks were made of normal concrete. Pockets/holes of the slab were filled with non-shrinkage high strength grout. Table 2 lists the material properties used for the test.

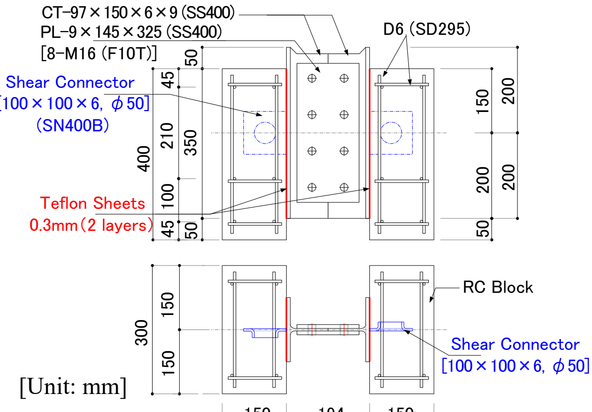

(a) Specimen BR-N

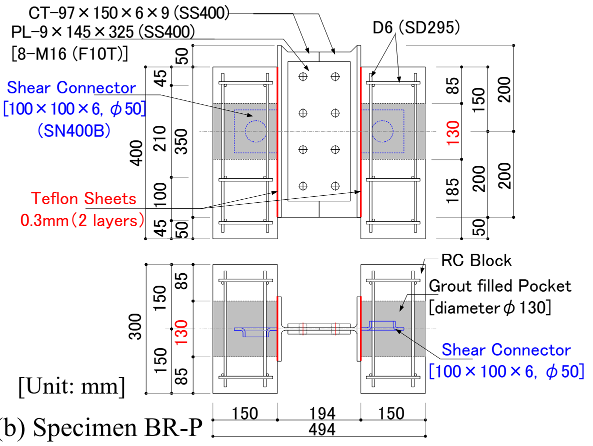

(b) Specimen BR-P

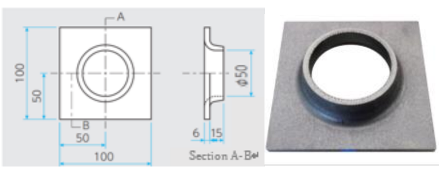

(c) Shear connector

Fig.2 Outline of tested specimens

Table 1 List of test specimens

Construction type	Specimen	Loading type
Conventional	BR-N-1	Monotonic
	BR-N-2 & BR-N-3	Cyclic + Monotonic
Precast	BR-P	Monotonic
	BR-P-2 & BR-P-3	Cyclic + Monotonic

2.2 Loading and instrumentation

Vertical loading setup used in the test and loading pattern are shown in Fig.3. Specimens were simply set on the rigid steel base of the testing machine by a thin layer of gypsum (gap filler), without any lateral restraints. Load was applied by a universal loading machine on the specimens' steel beam part. Whereas one specimen of each type was subjected to only a monotonic loading, a non-reversed vertical loading was planned for the other specimens, followed by a monotonic loading phase going beyond the nominal ultimate shear strength P_u of the shear connector ($P_u = A_s \times f_u/\sqrt{3}$, where A_s and f_u are, respectively, the cross section and ultimate strength of the shear connector) until the relative displacement would reach 10 mm. Each loading cycle was performed 5 times to apprehend the effect of loading cycles. As considering grout shear failure not occurring on the sides of the burring part due to the high strength of grout, connector's yield strength would develop, then the amplitudes of the loading cycles were related to the shear connector's nominal yield shear strength P_y ($P_y = A_s \times f_y/\sqrt{3}$, where f_y is the yield strength of shear connector). Amplitudes were, successively, $F_1 = P_y/3$, $F_2 = 2P_y/3$ and P_y.

Total displacement of the loading plate at the top of the specimen and relative displacements (horizontal and vertical) between the flange of steel T-beams and concrete blocks at the mid-level of the shear connector were measured using displacement transducers (Fig.4).

Table 2 Characteristics of materials

Cement.material	E_c (MPa)	f_c (MPa)	f_t (MPa)
Concrete	21,600	20.0	2.04
Grout	19,700	50.3	4.07
Steel material	E_s (MPa)	f_y (MPa)	f_u (MPa)
CT beam	NA	336	447
Connector	NA	333	445

Note: E_c, E_s: Young's Modulus, NA: not available, Poisson ratios of concrete and grout NA. f_c: compressive strength, f_t: tensile strength, f_y: yield strength, f_u: ultimate strength

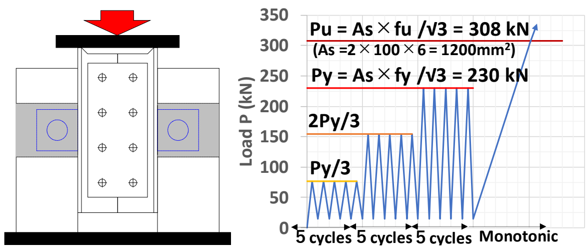

Fig.3 Outline of load setup and loading protocol

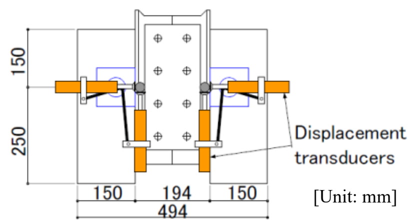

Fig.4 Outline of displacement transducers set

2.3 Test results

Figure 5 and Table 3 show the main test results of all tested specimens. Discontinuous lines in Fig.5 present the nominal shear strength values (P_y and P_u). Fig.6 and Fig.7 illustrate, respectively, the typical crack pattern in concrete at the end of loading and deformed shape of shear connectors after removing the concrete part. For all test specimens, the load increased considerably within a small displacement range, and stiffness consistently decreased when loading reached the nominal value P_y. Then, deformation progressed as load increased, and the experiment was ended with an insignificant load decrease in specimens BR-N, whereas in specimens BR-P, maximum load was reached when relative displacement was around 4mm, then the load gradually decreased, and the test was terminated.

No brittle failure was observed during testing. Based on the deformation state of the shear connectors at the end of loading (Fig.7) and the results of the FE analysis that will be presented in Section 3.4, the authors believe that, for all specimens, the shear connectors have undergone a combined shear yield-bearing failure mode. Focusing on the performance of specimens BR-P, their average initial stiffness and maximum load were, respectively, 1.59 times and 1.1 times those of specimens BR-N. Also, at similar load levels (Fig.5(b)), the relative vertical displacement of specimens BR-P before P_y or even when reaching P_u was less than half that of specimens BR-N. This can be explained by the high bearing capacity of grout in comparison to that of concrete (using material properties of Table 2, the bearing capacity of grout based on Ollgaard et al. [5] is $0.5 \cdot \sqrt{(f_c \cdot E_c)} = 497.7$ MPa while that of concrete is 328.6 MPa). At the interface concrete-shear connector of specimens BR-N, concrete underwent gradual crushing earlier than grout at the interface grout-shear connector of specimens BR-P, and consequently deformation within specimens BR-N was larger and shear strength at yielding of the shear connectors in the specimens BR-P was reached at smaller displacement. Higher values of the maximum load of specimens BR-P are deemed to the high shear capacity of the grout part that crosses the hole of the shear connector, in combination to its high bearing capacity, and to the cylindrical form of the grout part that helped reduce the stresses transferred from the shear connector to concrete and then delaying the development of the splitting cracks in concrete.

Test results showed the suitability of the precast connection (BR-P) in terms of structural performance, compared to that of the cast-in-place connection (BR-N). Also, the strength degradation in specimens BR-P was small, where the residual strength at a large deformation was more than 85% of the maximum load, proving the ductile behavior of the proposed connection. Also, the cyclic loading at different load levels, though of small number of cycles, indicated that the precast connection would provide better fatigue resistance, ultimately delaying collapse of such system caused by a structural damage or an extreme load exceeding the design value.

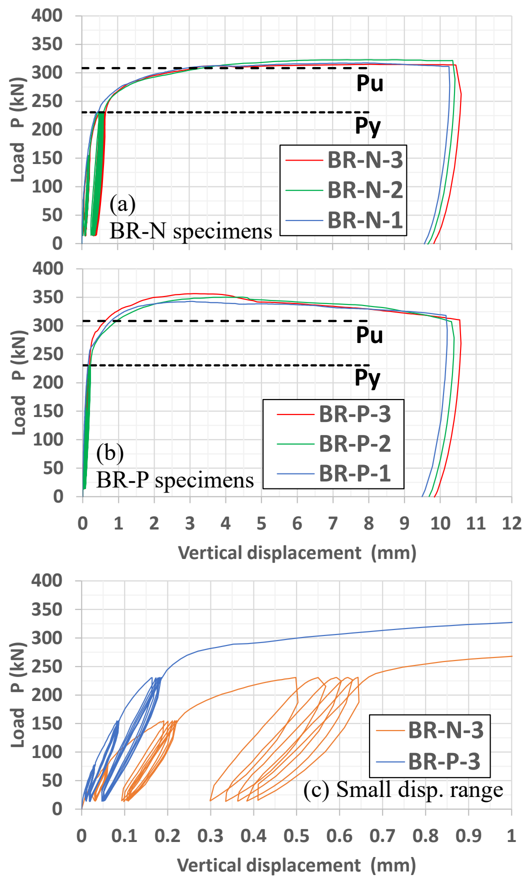

Fig.5 load – relative vertical displacement curves

Table 3 Main test results

Specimen	K_i (kN/mm)		$P_{max.}$ (kN)	
BR-N-1	1515.4	Aver. 1437.3	317.3	Aver. 318.3
BR-N-2	1562.1		322.9	
BR-N-3	1234.4		314.8	
BR-P-1	2467.3	Aver. 2287.5	343.0	Aver. 349.9
BR-P-2	1969.3		350.3	
BR-P-3	2426.0		356.4	

Note: K_i: initial tangent stiffness, Aver.: average value, $P_{max.}$: maximum recorded load

3. FINITE ELEMENT ANALYSIS

3.1 Model, loading and boundary conditions

The outline of the 3D FE model (half-model adopted owing to symmetry) is depicted in Fig.8. The

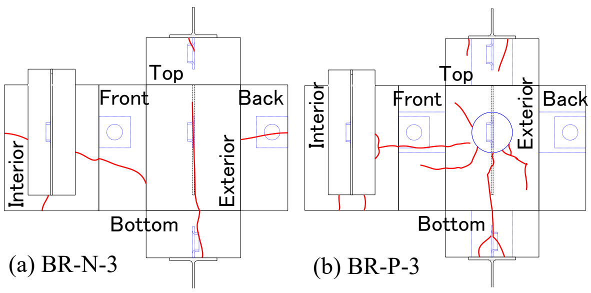

(a) BR-N-3 (b) BR-P-3

Fig.6 Examples of crack pattern at end of loading

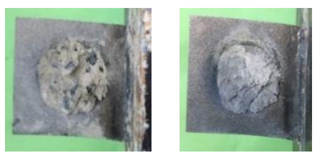

(a) BR-N-3 (b) BR-P-3

Fig. 7 Examples of deformed shape of shear connectors at end of loading non-linear analysis was conducted using the commercial software Ls-Dyna R11.1.0 [6]. Concrete, grout, steel T-beam, steel joint plates, shear connectors and steel base plate were modeled as solid elements where a relatively high-density mesh was used. The aspect ratio of solid elements was between 1.0 and 3.0. Steel reinforcing bars were explicitly modeled as beam elements incorporated into the concrete mesh. Bolts for joining the symmetrical parts (steel T-beams) of the specimens were not modeled, instead their resultant pressure was applied on both sides of the steel joint plates. The average clamping stress was 17 MPa, based on the applied torque on bolts.

Models concerned the tested specimens with the lower steel base plates (support reaction plates) and did not include the whole loading setup. The steel base plates on which the specimens were set were restrained against all movements (vertical and horizontal displacements and all rotations). Along the symmetry plane (vertical side of the steel joint plates), horizontal displacements and rotations were appropriately constrained, while the vertical displacement was not. Similar load conditions as in the test were reproduced in the models. Displacement-controlled monotonic loading was applied, in the downward direction, at the upper side of the flange of the steel T-beam. While the upper side of the flange was restrained in all horizontal directions, it was allowed to rotate around all three diagonal axes.

3.2 Material modeling

Material test data were used in the analyses. Continuous surface cap model (CSCM) was used for the constitutive material behavior for concrete and grout (Fig.9(a)~(c)). This cap model is characterized by a smooth and continuous intersection between the shear yield surface and hardening cap. For setting up the model input, in this study, default material parameters were requested based on the unconfined compressive strength and maximum gravel size as input. The derived Young's modulus, Poisson ratio and tensile strength of concrete are based on CEB-fib [7].

Plastic-kinematic model was used for the constitutive material behavior for steel plates and steel bars (Fig.9(d)). This elastic-plastic model is suited to model hardening plasticity. Whereas default material parameters were requested, the input values were Young's modulus (205000 MPa), the yield strength and tangent modulus.

3.3 Bond and interface modeling

Full bond was assumed between the steel bars and concrete, the shear connectors and the grout part, and the grout part and its surrounding concrete. To treat the interaction at the interface between concrete and steel T-beam flanges, tie-break surface contact elements were used. Whereas all surfaces which are initially in contact have normal and shear components, both were set to zero (no tensile or shear initial strength, as shown in Fig.10). Then, the only needed input was the friction coefficient μ. As Teflon sheets were set between the concrete blocks and the flange of T-beams, the friction at that interface was taken as zero. For the interface between the concrete block and steel base plate, whereas an initial value of 0.6 was considered, based on the minimum value of the study carried out by Rabbat and Russell [8], to reach a better matching with the test results a lower value of 0.3, based on the study of Bui et al. [9] was considered. As for the interface between the web of the T-beam and the steel joint plates, a high value of friction coefficient of 0.8 was considered after various trials in which other lower values [10, 11] were not satisfactory.

3.4 Analysis results

For both models, analysis was carried out beyond the maximum load, until the displacement reached the level achieved in the test. The numerical results of the models in terms of shear force and relative vertical displacement between the concrete block and T-beam flange (corresponding to the same locations in the test) are illustrated in Fig.11, and a summary of main results is presented in Table 4 simultaneously with the test results. Distributions of numerical strains of the models at the time of maximum load are illustrated in Fig.12 and Fig.13. It is worth to mention here that the numerical results were compared with the test results of the specimens that were subjected to monotonic loading (BR-N-1 and BR-P-1).

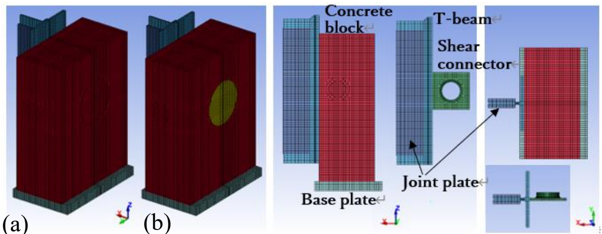

(a) Model BR-N (b) Model BR-P (c) Vertical view (d) Plan view

Fig. 8 Outline of numerical models

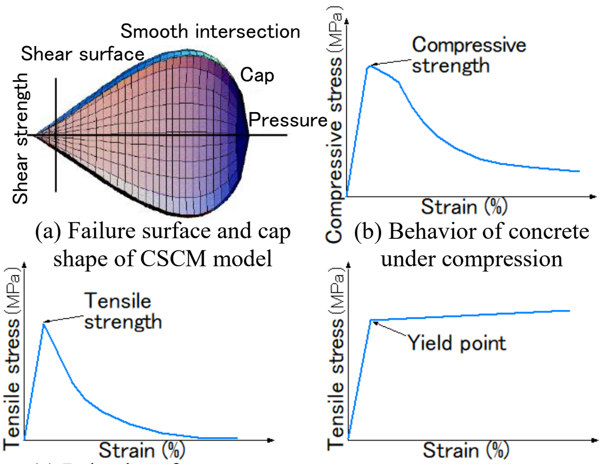

(a) Failure surface and cap shape of CSCM model (b) Behavior of concrete under compression

(c) Behavior of concrete under tension (d) Behavior of steel

Fig. 9 Outline of material models

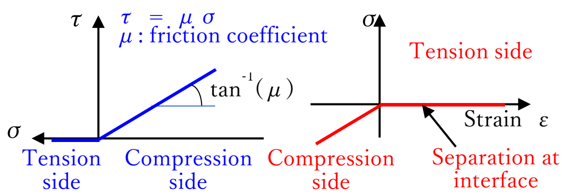

Fig. 10 Behavior of contact model for interfaces

The selected input values of different parameters of the analysis seemed very appropriate for both models, as the numerical results were satisfactory in terms of force, displacement and strain distribution. The analyses showed that the resulting load-displacement curves were reasonably close to those of the test, even at relatively large deformation, as illustrated in Fig.11. Furthermore, the distribution of the numerical maximum principal strains was reasonably compatible with the crack pattern observed on the corresponding tested specimens, as shown in Fig.12. Like in the test, the model BR-P was stiffer and had higher strength than the model BR-N, as shown in Table 4. Whereas the numerical initial stiffness of the model BR-P almost matched the test value, that of the model BR-N was 15% lower than the test value. Whereas the numerical maximum load of both models matched the test values, the deformation at which occurred the maximum load of the model BR-P was 25% higher than the test value and that of the model BR-N was 17% lower than the test value.

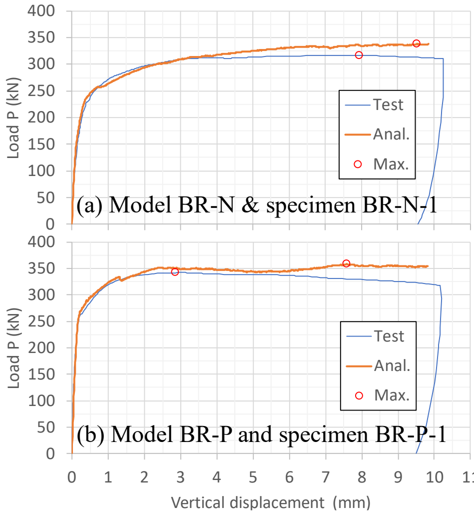

Fig. 11 Comparison of load-relative vertical displacement curves from test and analysis

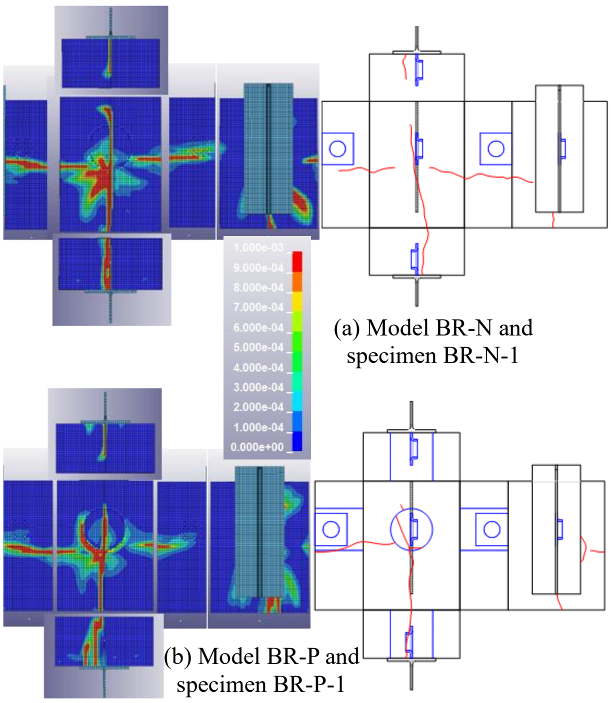

Fig. 12 Comparison of maximum principal strain distribution of concrete block at maximum load and crack pattern at end of loading

Similarly in both models, the failure mode was characterized by a combined bearing-yielding failure (yielding of plate of the shear connector and bearing failure on the interface concrete-shear connector for the model BR-N or grout-shear connector for the model BR-P), then elaborated by splitting cracks in the concrete blocks (Fig.12). The high-bearing capacity of grout in contact with the shear connector resulted in concentration of deformation at the base of the shear connector (part close to the flange) of the model BR-P, as it can be seen through the strain distributions in Fig.13. In the contrary, for the model BR-N, the low-

Table 4 Main test results

Model	K_i (kN/mm)			$P_{max.}$ (kN)		
	Test	Anal.	T/A	Test	Anal.	T/A
BR-N	1515.4	1776.5	0.85	317.3	338.6	0.94
BR-P	2467.3	2376.1	1.04	343.0	352.2	0.97

Note: K_i: initial tangent stiffness, $P_{max.}$: maximum load., T/A: Test/Analysis

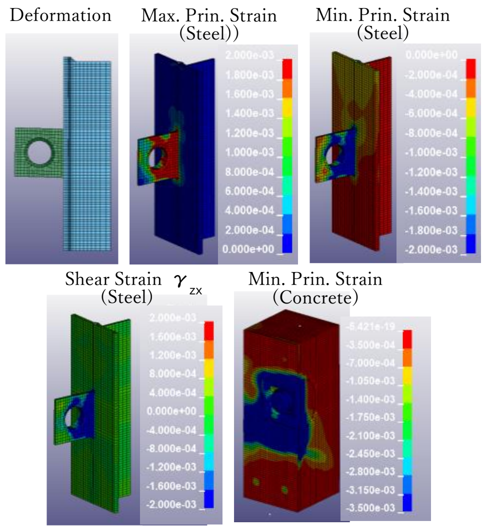

(a) Model BR-N

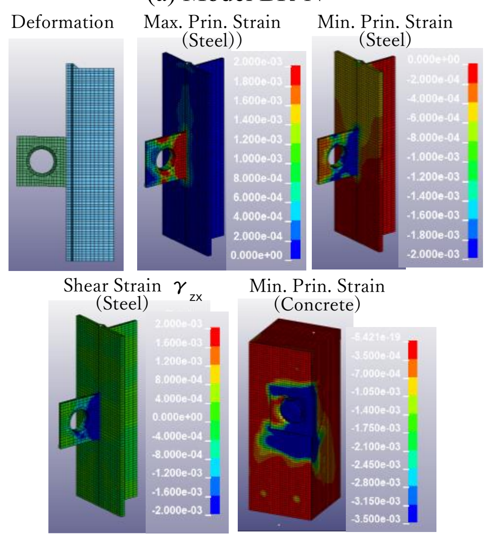

(b) Model BR-P

Fig. 13 Comparison of deformations, strain distributions in steel parts and inside concrete at maximum load bearing capacity of concrete in contact with the shear connector resulted in a deformation of the shear connector beyond its base (part close to the flange including the part with the hole), as it can be seen on the same figure. The analysis showed that the grout part was effective and improved the performance of the connection, and, in total, the analysis could fairly reproduce the global behavior of both specimens. Therefore, some discrepancies can still be noticed at some parts of the curves and between the crack pattern and maximum principal strain distribution, due to some reasons more likely: ①non-uniformity in the actual friction on every interface and non-similarity on all considered interfaces, especially for parts subjected to confining stresses, ②the mesh size and variation of the size ratio conditioned mainly by the form and size of both the grout part and the shear connector, and ③some deformation discrepancies at the fixation of the symmetrical parts on each specimen which might have induced some difference in movement when loading was carried at the top of the flanges (contrary to the analysis in which all the top of the flange in the model moved simultaneously all together). Whereas more accurate results would be expected by a more refined analysis, the presented one seems encouraging as it could predict the failure modes and provide acceptable strength values.

4. CONCLUSIONS

This paper briefly presented a demountable/reusable floor system composed of steel beams and precast RC slabs using burring-process perforated steel plates as shear connectors. In this paper, as a preliminary study, only the connection was examined by comparing the conventional practice of the mentioned shear connectors when embedded directly in a concrete slab to the case when embedded in grouted pockets made in the slab. This study investigated, experimentally by push-out tests and numerically by FE modeling, the composite behavior of such shear connectors under static shear loading. The following findings can be drawn.

(1) For the specimens of both conventional and precast connections, the push-out tests showed that using the burring-process perforated shear connector did not result in a brittle failure or fracture of the shear connector under large deformations. Both construction methods can be used safely.

(2) The performance of the specimens of the precast connection proved to be more appropriate due to the positive effect of the grout pocket and would provide better fatigue resistance, which ultimately would delay collapse of such composite system caused by a structural damage or some extreme loads exceeding the design value.

(3) Unfortunately, simulation of the dismantling process of the concrete was not carried out as aimed for the proposed system, since the concrete blocks were cracked at completion of the test, then, coring of the grouted pocket was judged not significant.

(4) The numerical results of the elaborated models for both conventional and precast connections were satisfactory and, in total, could fairly reproduce the global behavior of both types of tested connections.

(5) Whereas the presented analysis seems encouraging as it could predict the failure modes and provide good strength values, some small discrepancies still exist between test and numerical results. More accurate results are expected by a refined further analysis.

(6) Behavior of a full beam and slab jointed at multiple locations using the burring-process perforated steel plates (shear connectors) will be investigated numerically considering the parameters of the present study.

REFERENCES

[1] Sitepu, M.H., Matondang, A.R. and Tryana, M., "Sustainability Assessment in Construction Industry Supply Network: A Review," IOP Conf. Series: Materials Sci. and Eng., 725, 012032, 2020.

[2] Tadros, M.J., Badie, S.S. and Kamel, M.R., "Girder/Deck Connection for Rapid Removal of Bridge Decks," PCI Journal, 47(3), pp.58-69, 2002.

[3] Maruyama, Y., Tanaka, T. et al., "Experimental Study on Joint between Steel Beam and Concrete Slab Using Burring Shear Connector," 14th Symp. on Research and Application of Hybrid and Composite Structures, AIJ and JSCE, 2021.

[4] Figueira, D., Ashour, A., Yildrim, G., Aldemir, A. and Sahmaran, M., "Demountable Connections of Reinforced Concrete Structures: Review and Future Developments," Structures, 34, pp.3028-3039, 2021.

[5] Ollgaard, J. G., Slutter, R. G. and Fisher, J. W., "Shear Strength of Stud Connectors in Lightweight and Normal Weight Concrete," AISC Eng. J., American Inst.of Steel Constr., 71-10, pp.55-64, 1971.

[6] LSTC, "LsDyna R11.1.0: FE Code for Nonlinear Dynamic Analysis of Structures," Livemore Software Technology Corporation, 2019.

[7] CEB-fip, "CEB-fip Model Code 1990," Comité Euro-International du Béton, Thomas Telford House, 1993.

[8] Rabbat, B. G. and Russell, H. G., "Friction Coefficient of Steel on Concrete or Grout," ASCE J. of Struc. Eng., 111(3), pp.505-515, 1985.

[9] Bui, Q. H., Kabeyasawa, T. and Kabeyasawa, T., "An Experimental Study on Shear Friction Between Concrete Foundation and Bedding," Proc. of Architectural Inst. of Japan, Paper 20294, pp.587-588, 2012.

[10] Charsetad, H. and Khorsandijou, S. M., "Effect of Surface Roughness on Steel-Steel Dry Friction Coefficient," Journal of Mechanical Research and Application, 4(3), pp.45-56, 2012.

[11] Pijpers, R. J. M. and Slot, H. M., "Friction Coefficients for Steel to Steel Surfaces in Air and Seawater," Journal of Physics: Conference Series, 1669-012002, 2020.